Phase separation and dynamic patterning in $Cu_{1-x}Co_x$ films under ion irradiation

P. Krasnochtchekov, R. S. Averback, and P. Bellon
Department of Materials Science and Engineering, University of Illinois at Urbana-Champaign, 104 South Goodwin Avenue, Urbana, Illinois 61801, USA

(Received 2 February 2005; revised manuscript received 21 July 2005; published 4 November 2005)

Phase separation behavior in thin $Cu_{1-x}Co_x$ films under irradiation (1.8 MeV Kr^+ ions) at different temperatures has been systematically studied for $0.10 \leqslant x \leqslant 0.20$. The development of phase separation in irradiated films (estimates of the average size of Co precipitates and concentration of Co in solution) was monitored using magnetic measurements. Analysis of magnetization data in the framework of superparamagnetic theory has shown that at irradiation temperatures $T \leqslant 330$ °C, phase separation in Cu–Co films of all compositions stabilizes at high doses ($\approx 1 \times 10^{16}$ cm^{-2}), indicating the existence of temperature-dependent dynamic steady states. At temperatures higher than ≈350 °C, indications of thermodynamic-like coarsening are observed. Below ≈300 K FC/ZFC (field-cooled/zero-field cooled) measurements clearly show the randomizing effect of irradiation. The observed phase separation behavior of Cu–Co system under irradiation agrees qualitatively well with kinetic Monte Carlo simulations performed in this work and with theoretical predictions of phase evolution in irradiated immiscible alloys.

DOI: 10.1103/PhysRevB.72.174102 PACS number(s): 61.80.Jh, 05.65.+b, 05.70.Ln, 75.75.+a

I. INTRODUCTION

Engineering alloys are traditionally processed by first exciting them above their ground states and quenching them into a metastable or even unstable configuration. Then, using time and temperature as process variables, the alloys are relaxed into their desired states. For nanotechnology applications, recent examples of this approach include the formation of precipitates in host matrices by combining either ion implantation or vapor condensation of immiscible alloy components with subsequent thermal annealing.[1,2] A scheme has been proposed where external driving forces are applied to the system as it undergoes thermal relaxation.[3–5] The driving forces in this scheme impose sustained fluxes of energy and mass between the material and its environment. In such dissipative systems, a delicate balance is established between the externally imposed dynamics and the internal dynamics of the material, and this balance controls the structural evolution of the material. By varying the relevant parameters during the processing, one can alter the competition between these dynamics and thereby controllably induce dynamical transitions from one steady state to another.[6] This general concept of driven systems applies to a wide range of processing conditions, such as ion implantation, ball milling, wear, ion sputtering, and others, as has recently been reviewed.[7]

A generic property of such driven materials is that they often self-organize into patterns with nanometer length scales. The precise length scale, moreover, is determined by the nature and intensity of the driving forces. It has been shown that the origin of this self-organization derives from the different length scales at which the competing internal and external dynamics are operating: short-range jumps of point defects by thermally activated diffusion (internal dynamics), and long-range forced (ballistic) jumps, such as in displacement cascades or sheared regions, which induce atom relocations over distances ranging from some tenths to several nanometers (external dynamics).[8] While the foundations for the theory describing this behavior are now established, it is presently unknown whether these idealized models are sufficiently robust to describe the behavior of even simple binary alloys, much less, complex engineering materials. One systematic study on ball milling of Ag–Cu alloys shows good qualitative agreement with the model,[9] however, quantifying the control variables has not been possible in such studies. The goal of the present work is to provide a systematic test of the predictions of this theory in a situation where the driving forces are reliably characterized, viz. ion beam irradiation. For this study we also employ a model alloy system, Cu-rich, Cu–Co alloys, which has long been employed for basic studies of precipitation behavior.[10] The system is particularly useful here since Cu and Co have very similar atomic sizes so that they form coherent precipitates. This greatly facilitates comparison with our kinetic Monte Carlo simulations on a rigid lattice.

The method employed here for testing the model calculations is illustrated by the schematic, dynamical phase diagram in Fig. 1. This diagram represents an alloy system such as Cu–Co, and shows the phase behavior as a function of two dynamical variables, the ratio of ballistic jumps to thermally activated jumps γ and the relocation distance R. Temperature, pressure, and composition are held constant. Ballistic jumps in this theory refer to the random displacements of atoms that occur during the energetic displacement process in cascades. For alloys that form miscible liquids, such as Cu–Co, it also includes the random jumping of atoms in the thermal spike phase of a cascade. The relocation distance in this theory refers to the distance that an atom is displaced during one displacement cascade. For a specific alloy composition, ion projectile and ion energy, the relocation distance is very nearly independent of temperature.[11,12] Thermally activated jumps refer to the atomic motion that occurs during chemical interdiffusion at the ambient temperature of the sample; in metals these jumps are mediated by point defects. In an irradiation environment, the defects created by the irradiation, itself, dominate the thermally activated diffusion process.

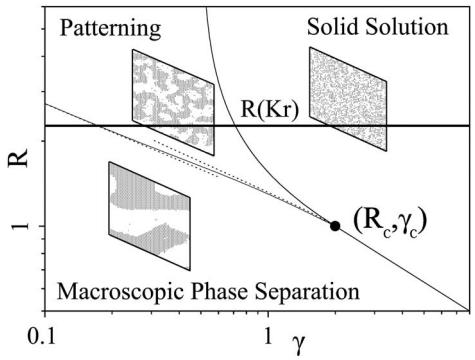

FIG. 1. Steady-state regimes of an immiscible $A_{50}B_{50}$ alloy as a function of the forced relocation distance R and the relative ballistic jump frequency γ. Horizontal line $R=R(\mathrm{Kr})$ schematically shows the phase-probing trajectory when the temperature is varied. Insets are (111) sections of actual three-dimensional kinetic Monte Carlo simulations. Adapted from Ref. 4.

We test the validity of the dynamic phase diagram in Fig. 1 in this work by varying the parameter γ while keeping constant the other control variable R. This is indicated by the dashed lines in Fig. 1. We can move along the line in Fig. 1 by either changing the irradiation flux or the irradiation temperature; the former changes the frequency of ballistic jumps and the thermally activated jumps (through the creation of point defects) while the latter varies predominantly the thermally activated jumps. We therefore chose to change the specimen temperature and assume that the small change in temperature required to dramatically change the number of thermally activated jumps does not much affect the ballistic jumps or the phase separation in the equilibrium phase diagram. The first assumption is well established for metals, in general. The second assumption is valid for Cu–Co, since the temperature range of interest is small. In addition, the large effect of temperature on radiation-enhanced diffusion in Cu is well documented.[13]

II. EXPERIMENTAL METHODS

$Cu_{1-x}Co_x$ samples with $x=10$, 15, and 20 were grown by sputter deposition with a typical base pressures of $\approx 3\times 10^{-8}$ Torr. Irradiations were performed with 1.8 MeV Kr ions using a Van de Graaff accelerator. The thicknesses of Cu–Co films in this study were ≈250 nm, which is less than the range of the Kr ions ≈300 nm. The deposited damage energy is, in fact, quite uniform, linearly increasing by ≈20% from the front to the back of the sample. Typical irradiation currents were 70–80 namps, which is sufficiently small to avoid beam heating. The base pressure in the target chamber was less than $\approx 2\times 10^{-8}$ Torr. Annealing of several sets of samples at temperatures up to 600 °C was performed using a high-temperature furnace with flowing Ar-2% H_2 gas. Analysis by Auger electron spectroscopy showed no evidence of segregation at the surface in the as-prepared, thermally annealed, or irradiated specimens.

The sizes of Co precipitates in Cu were determined from magnetization measurements within the widely used assumption of superparamagnetic response.[14,15] This analysis is based on the Langevin equation, although, simple corrections were included here to account for a distribution of cluster sizes. For thermal annealing studies, it is sometimes assumed that the precipitates sizes are described by a log-normal distribution, and in this case the average size and variance can be obtained from fits to experimental curves.[16] It is also possible, of course, to fit experimental curves using a sum of Langevin functions with each representing a different particle size.[17]

For the present study we will show through kinetic Monte Carlo (KMC) simulations that a log-normal distribution is a poor representation of the true size distribution of Co precipitates in Cu under ion irradiation. We therefore employ the second method. In our case we find that the experimental data are well fit assuming only two particle sizes. The total expression for the fitting function, therefore, was

$$M(H) = M_1[\coth(AN_1H) - 1/AN_1H] + M_2[\coth(AN_2H) - 1/AN_2H] + C, \quad (1)$$

where M_1 and M_2 are the values of total magnetizations of all particles with atomic sizes N_1 and N_2, respectively, and C is a constant representing a residual magnetization at zero applied field, i.e., the remanence. The remanence is usually associated with the "blocking" of individual particles. At 300 K, only Co particles larger than ≈12.5 nm in diameter become blocked, i.e., they contain more than $\approx 9\times 10^4$ atoms.[18] At 100 K, this number falls to $\approx 3\times 10^4$. For the two less concentrated alloys, blocking will be seen to have only small relevance in this work. The constant A in Eq. (1) is equal to μ_1/k_BT, where μ_1 is the moment of a single magnetic Co atom ($\approx 1.7\mu_B$). The volume averaged particle size and the saturation magnetization were calculated according to the formulas

$$\bar{N} = \frac{N_1M_1 + N_2M_2}{M_1 + M_2}, \quad (2a)$$

$$M_{\mathrm{tot}} = M_1 + M_2 + C. \quad (2b)$$

We use the volume average particle size since it best represents the physical measurements, i.e., many very small particles can strongly influence the numerical average size, but they have little effect on the magnetization, which is measured. This will be discussed in more detail, below. The Co atoms in solution do not contribute to the magnetization of the sample; therefore, a measurement of the saturation magnetization M_S relative to the total magnetization of the sample when all of the Co is precipitated M_T, i.e., M_S/M_T, yields information on the fraction of Co in solution. The magnetization measurements were performed between 5 and 300 K, using a SQUID 1 T magnetometer from Quantum Design. Reproducibility of particle size determination from magnetic measurements improves with increasing particle size, the error ranging from ≈5% for the larger sizes to ≈10% for the smaller sizes.

Finally we note two additional assumptions in Eq. (1), relevant to the current work. The first is that magnetic moment per Co atom is independent of the size of the Co precipitate. For precipitates smaller than ≈10 atoms, this as-

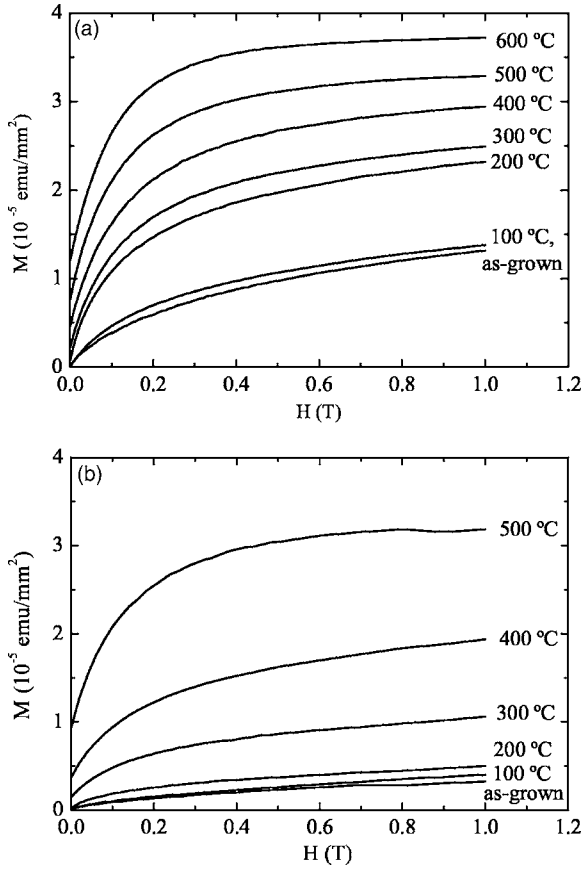

FIG. 2. Magnetization curves of $Cu_{90}Co_{10}$ samples annealed for 1 h at different temperatures: (a) as-grown and (b) preirradiated (5×10^{15} cm^{-2}) at RT (measurement at $T=100$ K).

sumption breaks down; however, since the precipitate sizes of interest here are much larger, this assumption introduces only an insignificant error. The second assumption involves magnetic (dipole-dipole) interactions between the particles. This effect is presently not well understood, and while it may lead to some uncertainty in the absolute sizes of the Co particles, less than ≈25% in precipitate diameter, we will show later that it does not influence the main conclusions of this work.

III. RESULTS

A. Effects of thermal annealing

Since our procedure requires varying the temperature of the specimen during irradiation, it was necessary to first characterize the kinetics of phase separation in our $Cu_{1-x}Co_x$ films during thermal annealing. These preliminary measurements also helped to identify the limitations of the superparamagnetic theory for the irradiation study. The $Cu_{90}Co_{10}$ and $Cu_{80}Co_{20}$ alloys, were employed for this part. The results for the magnetization behavior of the $Cu_{90}Co_{10}$ samples are shown in Fig. 2(a) as a function of annealing temperature in the range $T=100$ to 600 °C. The holding times at temperature were ≈1 h.

Two features in these data indicate that the as-grown films are not perfectly random alloys. First, the films have a significant magnetization prior to thermal annealing above room temperature, and second, annealing affects the magnetization at temperatures as low as 200 °C. Since bulk diffusion becomes significant only at higher temperatures, some Co must be located in grain boundaries, enabling it to precipitate at these low temperatures. The grain sizes of the samples were estimated from x-ray diffraction measurements using the Scherrer equation to be ≈25 nm, for both the $Cu_{90}Co_{10}$ and $Cu_{80}Co_{20}$ films.

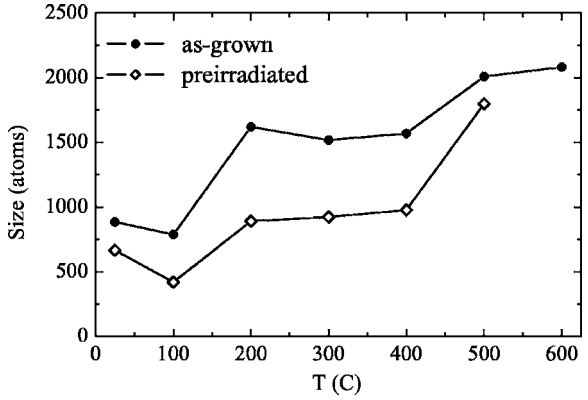

FIG. 3. Evolution of sizes of Co precipitates in $Cu_{90}Co_{10}$ samples with the annealing temperature for both as-grown (solid circles) and RT (5×10^{15} cm^{-2}) preirradiated (open diamonds) samples (measurement at $T=100$ K).

According to the theory of Martin,[19] and corroborated by a number of experimental studies,[12] alloy samples can be randomized by irradiation at sufficiently low temperatures. We therefore attempted to homogenize one set of $Cu_{90}Co_{10}$ samples by pre-irradiating them at room temperature, using an ion dose of 5×10^{15} cm^{-2}. Magnetization curves of the annealed samples from this set are shown in Fig. 2(b). The two expected results were achieved by preirradiation: the saturation magnetizations of the as-grown samples decreased substantially, and the onset of phase separation shifted to higher temperatures. Evolutions of the sizes of Co precipitates in as-grown and preirradiated $Cu_{90}Co_{10}$ films are shown in Fig. 3 as a function of annealing temperature. It is seen that preirradiation has made these samples more resistant to annealing for temperatures <500 °C; above 500 °C bulk diffusion becomes significant. The grain size in our films grew to ≈33 nm during irradiations to high dose, but it remained unchanged during thermal annealing.

The magnetization measurements of the $Cu_{90}Co_{10}$ samples reported above were all performed at $T=100$ K, rather than room temperature (RT), to increase the sensitivity of the magnetometer to the small precipitates in our small samples [see Eq. (1)]. Measurements were also performed, however, at RT. They show that for both the $Cu_{90}Co_{10}$ and $Cu_{80}Co_{20}$ samples, H/T scaling is not obeyed, with sizes determined at the lower temperature being approximately three times smaller [Figs. 4(a) and 4(b)]. We attribute these deviations to the magnetic dipole interactions alluded to earlier. These interactions become increasingly important with decreasing temperature.[20] The effect of blocking also becomes important in the $Cu_{80}Co_{20}$ at 100 K, as suggested by a large remanent magnetization (≈30% M_T) that was observed

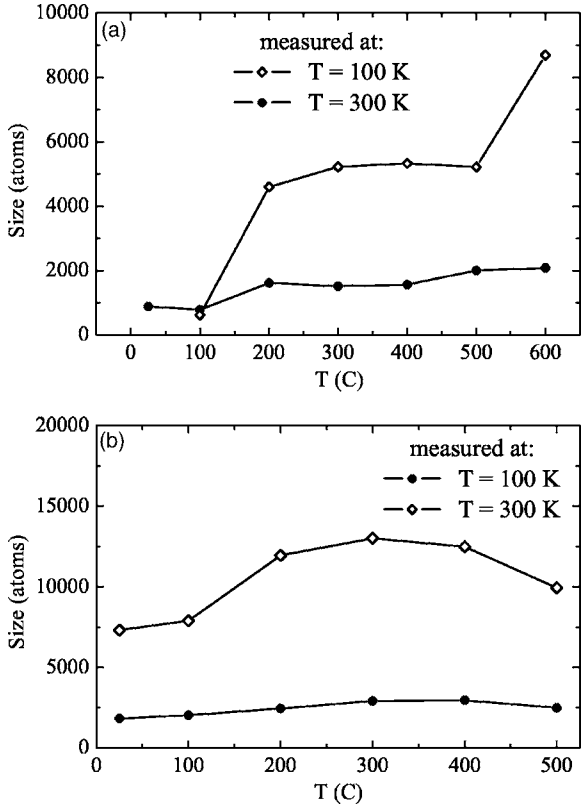

FIG. 4. Dependence of the sizes of Co precipitates on measurement temperature in annealed Cu–Co samples. $T=100$ K (solid circles) and $T=300$ K (open diamonds): (a) $Cu_{90}Co_{10}$ and (b) $Cu_{80}Co_{20}$.

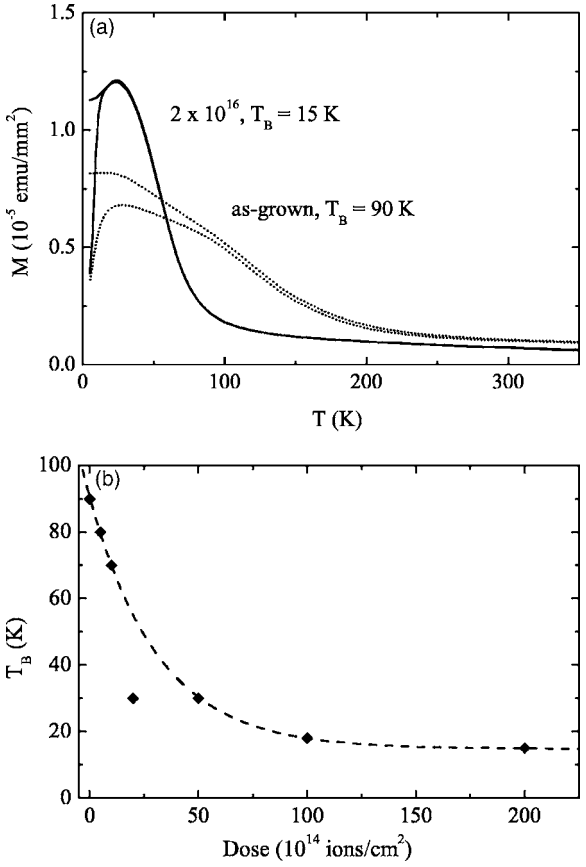

FIG. 5. (a) Examples of FC/ZFC curves for as-grown $Cu_{85}Co_{15}$ samples irradiated at RT and (b) the dependence of the maximum blocking temperature on dose.

in these samples. It should be noted that blocking can also give rise to a "too-small" apparent particle size distribution since only the smallest particles are unblocked [Fig. 4(b)]. Measurements of the $Cu_{80}Co_{20}$ samples at 100 K, therefore, will not be considered further.

An additional purpose of the thermal annealing measurements was to determine the saturation magnetizations of the samples after all of the Co atoms were in large precipitates M_T. This value serves as a check on the total content of Co in the samples. The values obtained were consistent with our estimates of total Co content in the films, using the accepted magnetic moment of 1.7 Bohr magnetons per Co atom. All films in this study were corrected for a small diamagnetic contribution from the Si/SiO_2 substrate.

B. Dissolution of Co precipitates in $Cu_{85}Co_{15}$ alloys by ion irradiation from FC/ZFC curves

Dissolution of Co precipitates at room temperature in as-grown $Cu_{85}Co_{15}$ samples was studied by determining the blocking temperature as a function of ion dose. The blocking temperature was obtained by acquiring magnetization data under conditions when specimen had been cooled either in an applied magnetic field, i.e., field cooled (FC) or in absence of a field, i.e., zero field cooled (ZFC). The temperature at which these curves diverge yields the maximum blocking temperature. As illustrated in Figs. 5(a) and 5(b), irradiation leads to a continuous reduction in the blocking temperature T_B starting at 90 K for as-grown samples, and decreasing to 15 K for samples irradiated to 2×10^{16} cm^{-2}. Based on the Bean-Livingston formula, which relates the size of precipitates V to the blocking temperature T_B via an anisotropy constant K_A, $K_AV\approx25\times k_BT_B$, we interpret the reduction in the blocking temperature as direct evidence for irradiation-induced dissolution of Co precipitates. The peak in the magnetization data at 15 K concerns the magnetic glass transition in this alloy, but since it is not relevant to understanding the present work, it will not be discussed further, here.

C. Ion irradiation of $Cu_{1-x}Co_x$ samples with $x=10$, 15, and 20

1. $Cu_{90}Co_{10}$

The irradiation studies on $Cu_{90}Co_{10}$ employed samples with three different initial microstructures: as-grown, preirradiated, and preannealed samples. The purpose of studying these different samples was to test the theoretical prediction that the long term patterning structure of irradiated alloys was independent of the initial alloy microstructure. Preirradiation, which was performed to randomize the alloys, consisted of an irradiation dose of 5×10^{15} cm^{-2} at RT. Preannealed samples were obtained by annealing at $T_A=500$ °C for one hour.

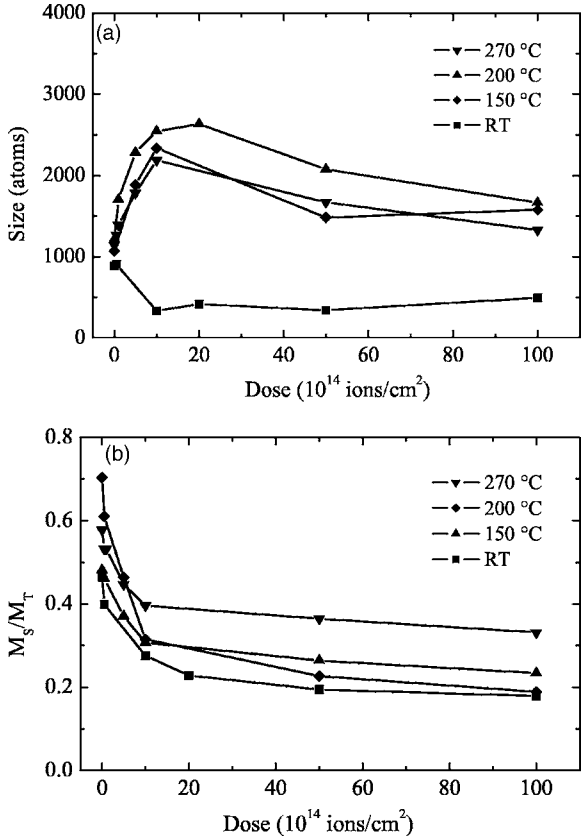

FIG. 6. Irradiation of as-grown $Cu_{90}Co_{10}$ samples at different temperatures: (a) particle sizes and (b) normalized magnetizations. Measurement at 100 K.

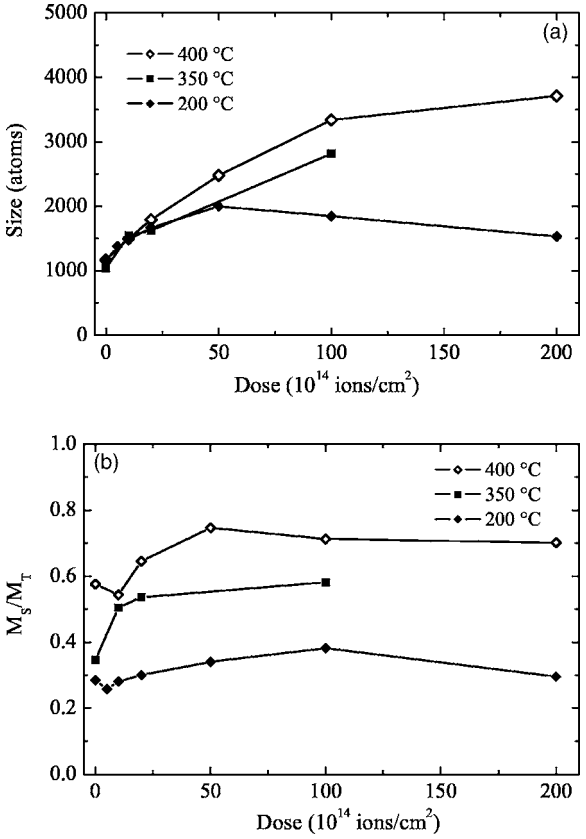

FIG. 7. Irradiation of preirradiated $Cu_{90}Co_{10}$ samples at different temperatures: particle sizes (a) and normalized magnetizations (b). Measurement at $T=100$ K.

The results for the as-grown $Cu_{90}Co_{10}$ samples measured at 100 K are shown in Fig. 6 for a series of irradiation temperatures. For a given temperature, all of the samples, including the unirradiated one, were held at the irradiation temperature while the irradiations were performed. Thus all of the samples at a particular temperature have been held at the irradiation temperature for the same length of time. For this reason, the microstructure of the unirradiated samples varied somewhat since they were held at different irradiation temperatures, and some thermal annealing occurred. On the whole, however, the data show a convergence of both the average sizes of Co particles and magnetizations to steady state values. The steady states, however, depend on the irradiation temperature. This trend is particularly clear for the normalized saturation magnetizations M_S/M_T which approach a steady state by a dose of $\approx 2\times 10^{15}$ cm^{-2}. The small decreases in M_S/M_T at higher doses can be accounted for by the loss of Co atoms from sputtering.[21]

Unlike the magnetizations, the average sizes of the Co particles do not approach their steady-state values monotonically, but rather they show significant transient effects. For the higher temperature irradiations, the average particle sizes increase to about twice their initial values, before decreasing toward the steady state value. By a dose of 1×10^{16} cm^{-2}, the average particle sizes become almost constant. This transient presumably derives from the broad range of precipitate sizes in the as-prepared samples, large precipitates at grain boundaries, and small precipitates in the grain interiors. During irradiation, the small particles dissolve quickly, relative to the larger particles, initially increasing the average particle size. Only at later times, when the larger particles at the grain boundaries dissolve, does the system come into a global steady state. This explanation is supported by the monotonic reduction in total magnetization. We are uncertain why this transient behavior is not observed in the specimen irradiated at room temperature, but since this sample was not thermally annealed, there are presumably fewer large precipitates (see Fig. 4), and thus a more uniform initial size distribution.

Results for the evolutions of the average particle sizes, and saturation magnetizations during irradiation of the preirradiated (randomized) samples at 200, 350, and 400 °C are shown in Figs. 7(a) and 7(b). The data for the sample irradiated at 200 °C do not show the strong a transient effect observed for the as-grown samples, presumably because the large grown-in precipitates were dissolved during the preirradiation treatment at room temperature. The steady state microstructure of this sample, on the other hand, is similar to that of the as-grown sample undergoing similar irradiation conditions; this is indicated by both the "steady state" values of the average particle sizes and the saturation magnetizations.

The films irradiated at $T=350$ and 400 °C behave quite differently from the others, appearing to be in the regime of driven, macroscopic phase separation. This is indicated primarily by the continued growth in particle size at these tem-

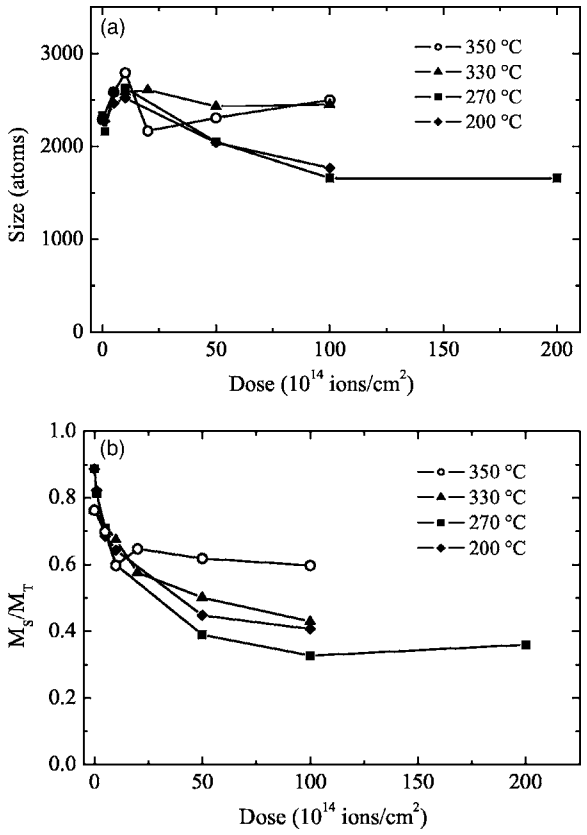

FIG. 8. Irradiation of preannealed $Cu_{90}Co_{10}$ samples at different temperatures: particle sizes (a) and normalized magnetizations (b). Measurement at $T=100$ K.

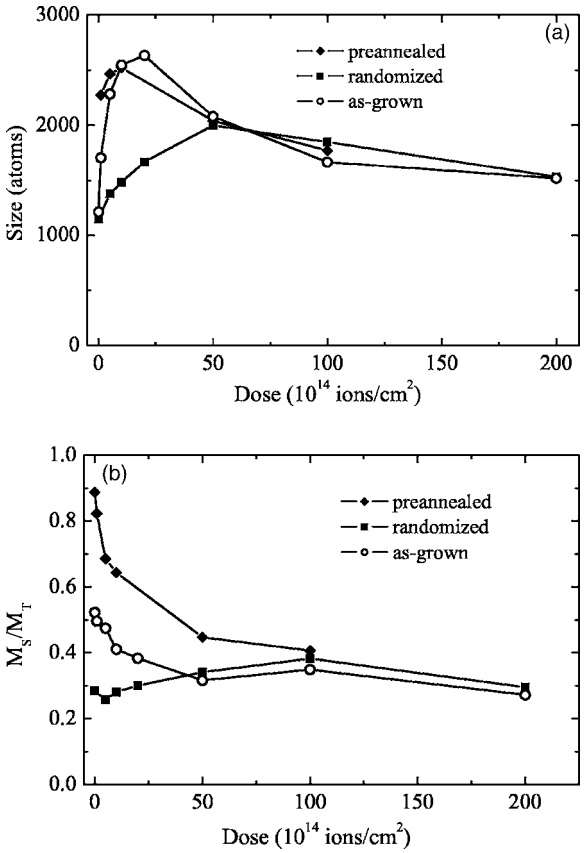

FIG. 9. Comparison of the evolution of particle sizes (a) and normalized magnetizations (b) with the dose at $T_i=200$ °C for three sets of samples: as-grown, preirradiated, and preannealed. Measurement at $T=100$ K.

peratures, showing no signs of saturation even after a dose of 2×10^{16} ions/cm^2. The maximum average particle sizes in these systems are ~3700 atoms.[22] Since no changes in the remanent magnetizations were found in these samples (data not shown here) even at the highest irradiation dose 2×10^{16} cm^{-2} and temperature $T=400$ °C, we can conclude that the effects of blocking are not important, which is as expected. Lastly, M_S/M_T in these samples irradiated at $T=350$ and 400 °C approach steady state values 0.6 and 0.7, respectively. This implies that a significant fraction of Co atoms remains in solution at these temperatures in dynamic equilibrium.

Prior to irradiation, the preannealed samples had an average particle size of ≈2000 atoms[22] and a saturation magnetization of $\approx3.0\times10^{-5}$ emu/mm^2 ($M_S/M_T=0.86$). These samples were irradiated at temperatures of 200, 270, 330, and 350 °C. Evolutions of the average particle sizes and magnetizations with dose are plotted in Figs. 8(a) and 8(b). These preannealed $Cu_{90}Co_{10}$ samples follow the same general trend as the as-grown and preirradiated samples. The only discrepancies in these measurements were slightly larger particle sizes and magnetizations for samples irradiated at $T=200$ °C than for samples irradiated at $T=270$ °C. The difference between the corresponding curves, however, is small and most likely derives from a small variation in the initial compositions of the films.

For irradiations at temperatures below a certain threshold temperature, the average particle size and magnetization appear to decrease to characteristic steady-state values, while above the threshold temperature, macroscopic precipitation begins, assisted by ion irradiation. While the irradiations of the randomized $Cu_{90}Co_{10}$ films indicate that the threshold temperature marking the transition between the regimes of microscopic patterning and macroscopic phase separation, is somewhat below $T_t^{\max}=350$ °C, the irradiations of the preannealed samples appear to narrow the possible range to $330\ °C<T_t<350$ °C. Indeed, while the average particle size at $T=350$ °C shows continuous growth, at $T=330$ °C the average particle size is already shrinking.

Finally, to support the assertion that regardless of their initial state, driven alloy systems with the same composition arrive at the same steady state, the dependencies on dose of average particle sizes and saturation magnetizations of our three types of $Cu_{90}Co_{10}$ specimens, as-grown, preirradiated, and preannealed, are plotted together in Fig. 9. For this comparison, data for the irradiation at $T=200$ °C are shown. It can be seen that there is a remarkable convergence for both particle sizes and magnetizations in these systems.

Up to this point, only results obtained by magnetic measurements performed at 100 K were reported. As indicated previously, better sensitivity is obtained at low temperatures. We tacitly assumed that while magnetic dipole interactions at 100 K may distort the absolute sizes of the particles, yielding sizes that are too small, they should not significantly affect

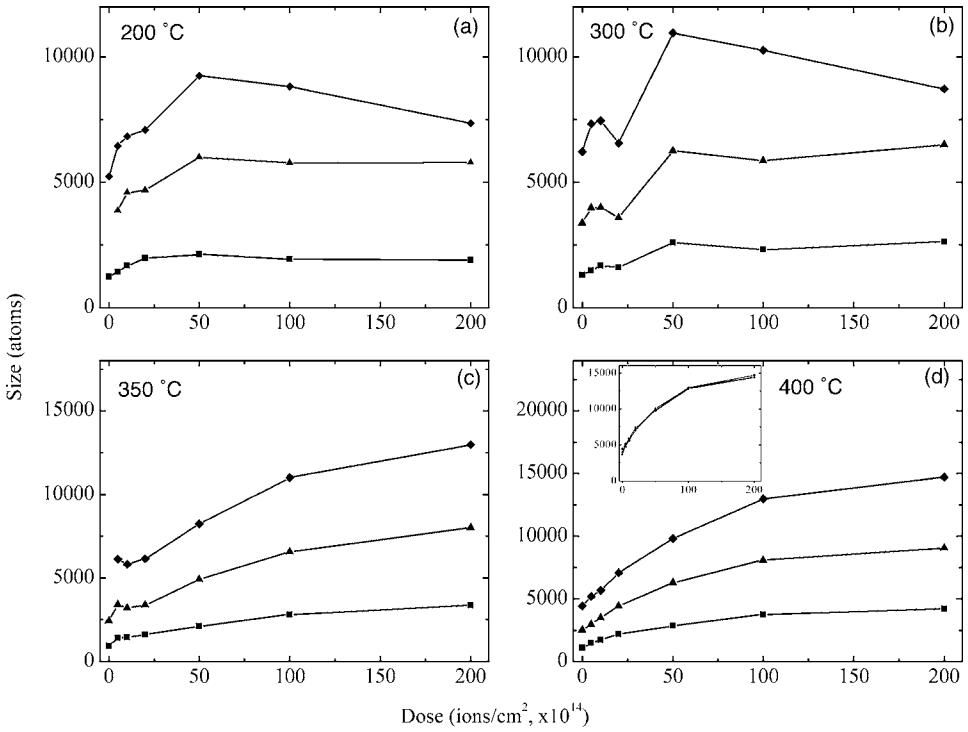

FIG. 10. Particle sizes of preirradiated $Cu_{90}Co_{10}$ samples irradiated at different temperatures and measured at $T=100$, 200, and 300 K. In the inset of (d) (400 °C) the curve for 100 K is scaled up by a factor of 3.4 and that for 200 K is scaled up by a factor of 1.6.

the relative sizes. To verify this assumption, we performed additional measurements at 100, 200, and 300 K on a second set of irradiated samples. These samples were all randomized by preirradiation at 300 K. The results are shown in Figs. 10(a)–10(d). Aside from a variation in the absolute values of size, the data are not sensitive to the measurement temperature. This is clearly seen in the inset of Fig. 10(d) for the sample irradiated at 400 °C, since the results of the measurements performed at different temperatures overlap when scaled by a simple multiplicative factor. Similar behavior is observed for the other irradiation temperatures. The data are thus related by a simple temperature-dependent scaling factor that is independent of the average size of the particle. We conclude, therefore, that while the average sizes of the particles are influenced by magnetic interactions, the trends that we have reported, are not.

2. $Cu_{85}Co_{15}$

Irradiations of $Cu_{85}Co_{15}$ films were performed at liquid nitrogen temperature (LNT), RT, 150, 200, 270, 330, and 400 °C. All samples irradiated at temperatures above RT were first randomized by preirradiation at RT. Average particle sizes and magnetizations calculated from the magnetic curves of these samples obtained at 100 K are presented in Figs. 11(a) and 11(b). The figures show that irradiations at LNT, RT, and 150 °C have driven the system to steady states, systematically varying in the values of the average particle size and saturation magnetization. At intermediate temperatures, 200 and 270 °C, it appears to require somewhat larger doses for the Co particles to equilibrate at their corresponding steady state sizes. Saturation magnetizations again equilibrate much faster than size distributions, which is expected since equilibration between large particles is slow compared to the initial stages of precipitation. Evolutions of the average particle size for irradiations performed at $T=350$ and 400 °C are again suggestive of macroscopic growth in particle size. By the highest dose of 2×10^{16}, the average particle size in irradiations at both temperatures reaches ≈3700 atoms.[22] While these measurements are useful for illustrating the systematic behavior, magnetic interactions again influence the absolute sizes. We therefore focus on the results obtained during measurement at 300 K.

The results of the magnetic measurements on the same $Cu_{85}Co_{15}$ samples, but now measured at 300 K, are shown in Figs. 12(a) and 12(b). Data for the same irradiation temperatures are shown. The particles sizes are not shown for irradiations at LNT and RT, since the magnetizations of the samples at high doses are too low ($<0.1M_T$) to obtain accurate values. It can be seen that the high temperature measurements yield qualitatively the same pattern of phase separation of $Cu_{85}Co_{15}$ films under ion irradiation as do the low temperature measurements, Figs. 11(a) and 11(b). Noteworthy in these data is the continued increase in particle size with dose for irradiation temperatures above ≈350 °C, again indicating that the system has crossed the boundary between patterning and macroscopic coarsening at a temperature above ≈300 °C. The growth of the precipitates appears somewhat slower in the measurements performed at 100 K; we will show in our discussion of absolute particles sizes, below, that this is likely due to the largest particles becoming blocked in the 100 K measurements. The low values of M_S/M_T for irradiations at RT and below illustrate that most of the Co is in solution. The somewhat larger values of M_S/M_T obtained for 100 K measurements is a consequence of the greater sensitivity of these measurements to the very small particles.

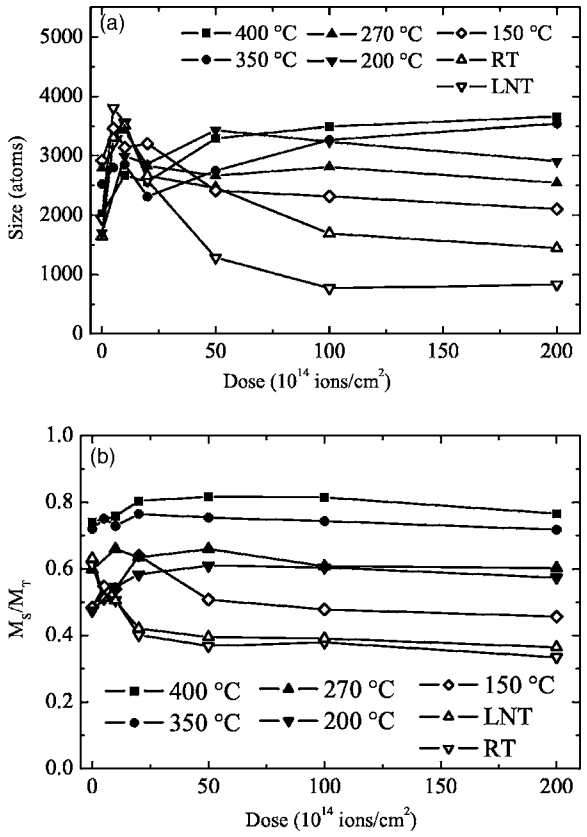

FIG. 11. Irradiation of preirradiated $Cu_{85}Co_{15}$ samples at different temperatures: (a) particle sizes and (b) normalized magnetizations. Measurement at $T=100$ K.

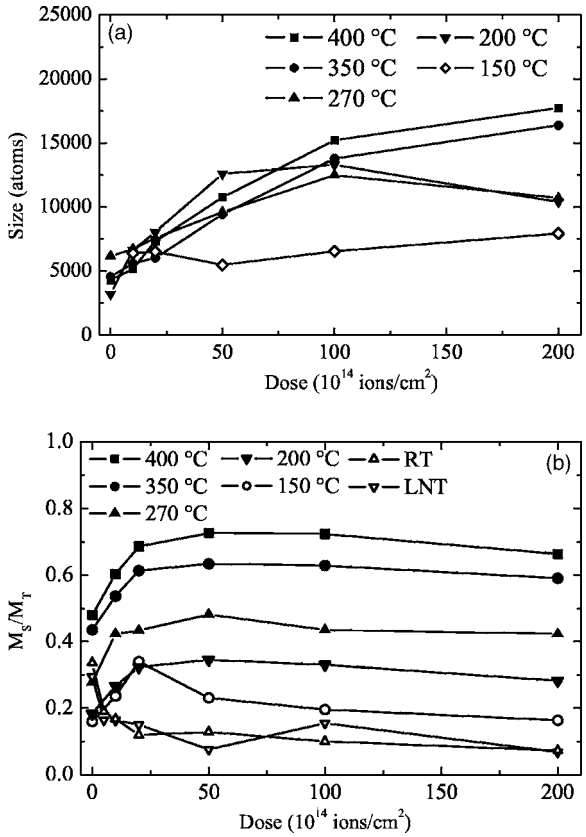

FIG. 12. Irradiation of preirradiated $Cu_{85}Co_{15}$ samples at different temperatures: (a) particle sizes and (b) normalized magnetizations. Measurement at $T=300$ K.

3. $Cu_{80}Co_{20}$

The data collected on $Cu_{80}Co_{20}$ are presented in Figs. 13(a) and 13(b). The samples irradiated at temperatures higher than RT were initially randomized by irradiation at room temperature. The range of irradiation temperatures for $Cu_{80}Co_{20}$ samples was LNT through 375 °C. As revealed by the annealing study of $Cu_{80}Co_{20}$ films [Fig. 4(b)], annealing at temperatures higher than 300 °C is already sufficient to produce many large precipitates that are magnetically blocked. Analysis of magnetization curves of $Cu_{80}Co_{20}$ samples irradiated above $T_i=270$ °C, indeed showed increased blocking. Therefore, evolution of the average particle size with dose is presented here only for samples irradiated at temperatures lower than 270 °C. On the whole, the particle sizes and magnetization data shown in Figs. 13(a) and 13(b) behave consistently with the previous results obtained for $Cu_{90}Co_{10}$ and $Cu_{85}Co_{15}$ samples. Perhaps due to a larger fraction of Co, $Cu_{80}Co_{20}$ samples approach steady states even faster than the $Cu_{85}Co_{15}$ samples. Evidence for the existence of steady states is strong for samples irradiated at the temperatures up to 200 °C. It is, however, not possible to determine the transition temperature between the patterning and macroscopic growth regimes for $Cu_{80}Co_{20}$ samples by our magnetization measurements, due to the strong particle blocking. On the other hand, the magnetization data show that even in this high concentration alloy, a significant fraction of the Co, 30%, goes into solution during irradiation at 375 °C. This value is quite similar to those found for the $Cu_{90}Co_{10}$ and $Cu_{85}Co_{15}$ samples.

D. Kinetic Monte Carlo simulations

Kinetic Monte Carlo (KMC) simulations have been performed on a model fcc binary alloy $A_{1-c}B_c$, to help to elucidate the experimental results. The heat of mixing of the alloy was chosen to be $\Delta H_m=7$ kJ/mol, which is similar to that of Cu-Co. In previous theoretical investigations,[3,8] we used KMC simulations to demonstrate that for such an alloy the dynamical competition between ballistic mixing induced by displacement cascades and thermally activated decomposition can force the stabilization of compositional patterns. That work showed that a first requirement for patterning is that the frequency of the forced atomic exchanges Γ be similar to that of the thermally activated atomic jumps. It is also required that the average atomic relocation range R exceed a threshold value R_c. These past studies, which led to the construction of Fig. 1, considered only the equiatomic composition. We have extended these calculations to the lower B concentrations; we report here the results for the 10% alloy.

The simulations were performed using a rhombic simulation cell containing 64^3 lattice sites. The average relocation distance was set to $R=1.73a_{NN}$, where a_{NN} is the nearest-neighbor distance. This value of a_{NN} was determined using molecular dynamics simulations of $Cu_{50}Ag_{50}$, irradiated with

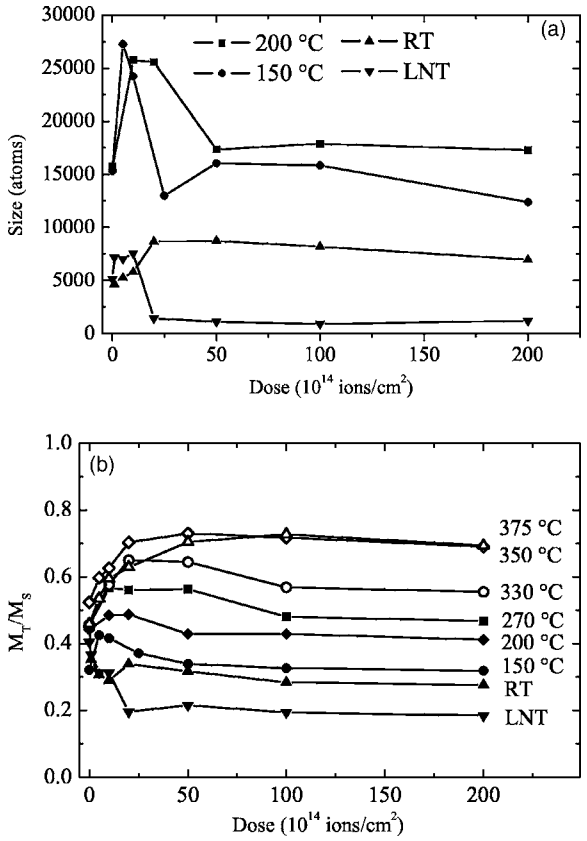

FIG. 13. Irradiation of preirradiated $Cu_{80}Co_{20}$ samples at different temperatures: (a) particle sizes and (b) normalized magnetizations. Measurement at $T=300$ K.

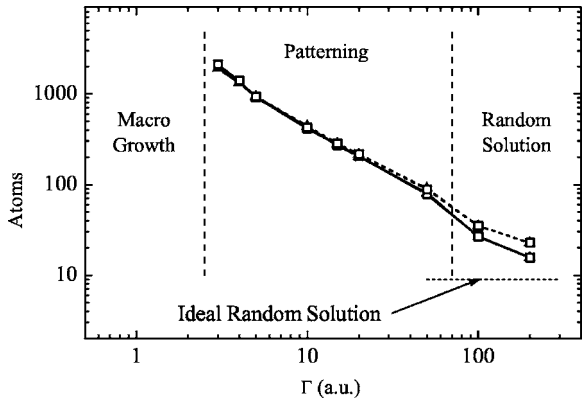

FIG. 14. Steady state sizes (volume-averaged) of *B*-rich particles in the patterning regime as a function of Γ (frequency of ballistic atomic relocations). Two sets of overlapping lines show sizes from two initial states: a random solution (triangles), and a precipitated phase (circles). Minimum cluster size is 5 atoms for the lower set of curves (solid lines), and 11 atoms for the upper set of curves (dash lines). The dotted vertical lines denote the boundaries between the macroscopic growth, patterning and random solution regimes, and the horizontal line shows the average cluster size (for clusters with five atoms and larger) for an ideal 10% random solution.

1 MeV Kr ions.[11] A similar value should hold for more dilute Cu-Co alloys irradiated with heavy ions. All other simulation parameters, as well as the kMC algorithm, are identical to those used in Ref. 8.

The low concentration of *B* atoms in the 10% alloy enabled us to measure the sizes of the *B*-rich precipitates in this system employing the Stillinger connectivity criterion for counting clusters, i.e., an atom is considered to belong to a cluster if it has at least one of its neighbors belonging to the cluster.[23] Sampling of the phase space was conducted by fixing the temperature at $T=200$ °C, and systematically increasing Γ. This method holds the rate of thermally activated jumps constant and therefore increases the ratio of the frequencies of ballistic and thermal jumps γ. The results of the simulations are summarized in Fig. 14, where the volume-weighted sizes of *B* precipitates at steady state as well as the boundary between the macroscopic growth and patterning regimes are plotted. In these simulations, two different initial states, a random solution and a thermally precipitated state, were used to make sure that the same steady state was obtained. This was indeed found, as illustrated in Fig. 14.

Patterning was identified in this work, as in Ref. 8, by the presence of a peak in the structure factor at a nonzero **k** wave vector. Beyond the crossover point between the macroscopic growth and patterning, evaluated at $\Gamma^* \approx 2-3$ s^{-1}, the system develops nanoscale compositional patterns. The microstructure of the alloy in steady state, shown in Fig. 15, includes both *B* precipitates and a large fraction of dissolved *B* atoms. It is noteworthy that while it is not known whether R_c is sensitive to composition, the same value of *R* that induced compositional patterning for $c=50\%$ (Ref. 11) was sufficient to produce patterns for $c=10\%$.

For the estimates of cluster sizes in Fig. 14, a minimum threshold cluster size has been introduced, i.e., clusters of

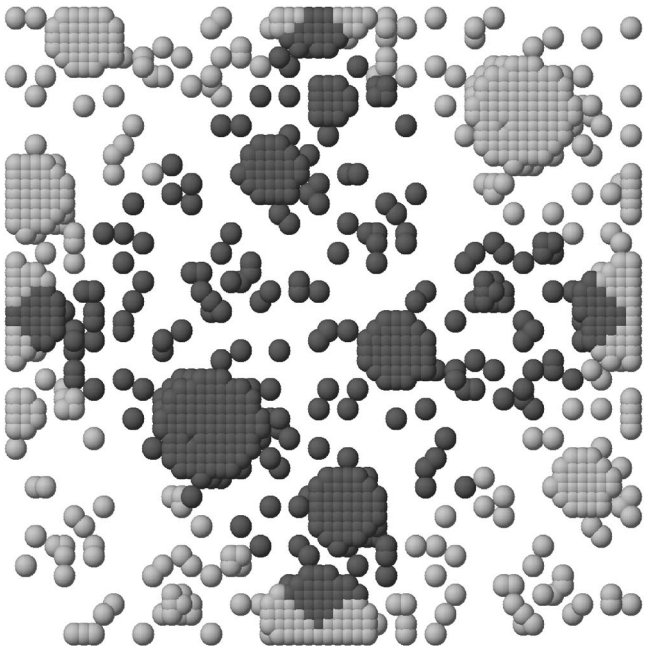

FIG. 15. Appearance of the steady state microstructure of $A_{90}B_{10}$ alloy under irradiation conditions given by $T=200$ °C and $\Gamma=3$. For better visualization, the system is shown with complemented boundary conditions, i.e., lighter colored atoms were added by translation of darker atoms across the boundaries.

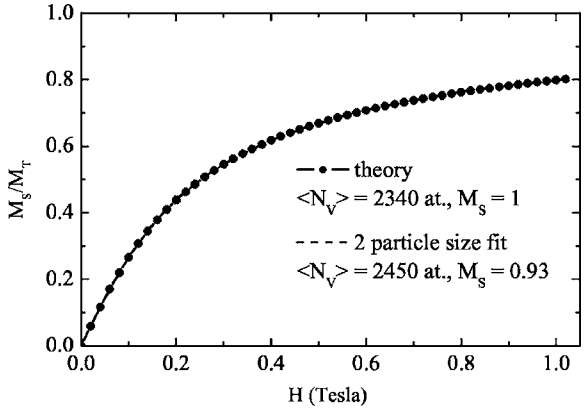

FIG. 16. Model superparamagnetic response of $Cu_{90}Co_{10}$ alloy with microstructure drawn from KMC simulations with T = 200 °C, and Γ = 3 (solid line with symbols), and the two-particle size fit to it (dotted line).

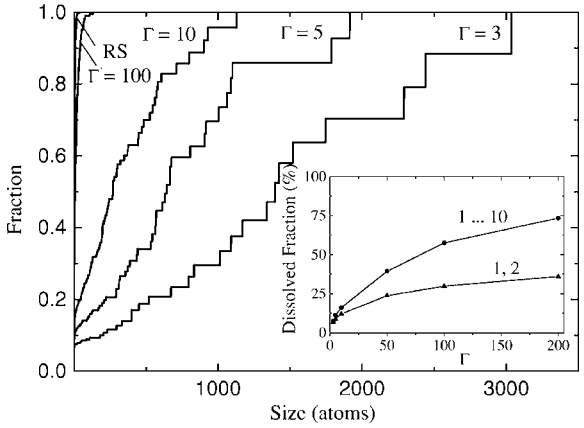

FIG. 17. Integral fraction of B atoms in clusters smaller than size n as a function of n for steady states reached at different relocation frequencies Γ. Curve RS represents the random solution. Initial values (at size equal to one atom) show the concentration of isolated B atoms (dissolved B). Inset: Variation of the steady state dissolved fraction with Γ considering cluster sizes up to 2 atoms or up to 10 atoms for the dissolved phase.

smaller size were not included. This threshold prevents random congregations of a few connected atoms in solution from being counted as a precipitate. For comparison, two sets of curves corresponding to a minimum cluster size of 5 or 11 atoms are plotted (Fig. 14). The curves nearly overlap, with only a small deviation at large Γ, where the cluster size is quite small. We employ the threshold of 5 atoms for the discussion that follows.

The precipitate size in the steady state microstructure is observed to gradually change from ~2500 at Γ=3 to ≈15 atoms at Γ=200. At $\Gamma \approx 70$ the curve for the average particle size exhibits a change in slope, which may be indicative of a phase transition from patterning to solid solution. For comparison, the volume-weighted average cluster size in an ideal 10% random alloy was calculated (shown with a horizontal dotted line in Fig. 14); it is ~8.9 atoms.

We also employed the simulations to check the validity of our use of two-particle size fits of magnetization curves used in the experimental part of this paper. For this purpose, theoretical magnetic response M(H) of our model $A_{90}B_{10}$ alloy system was first calculated using the actual distribution of B-rich particles obtained in the KMC simulations for T_i = 200 °C and Γ=3. As shown in Fig. 16 this curve agrees very well with the magnetization curve derived from a two-particle fit to the same simulation data. Of importance to this study is that the volume-averaged particle size (in atoms) is very nearly the same for the model curve N_V=2340 at., and for the two-particle size fit N_V=2450 at. The nonweighted average sizes, in contrast, are very different, with values of 640 at. for the model curve and 1730 at. for the two-particle size fit. A single particle size fit (not shown) also provided a good estimate of the volume-averaged particle size (2270 at.), however the quality of the fit was poorer and significant magnetization from smaller particles was lost (the loss of total magnetization was ≈12% compared with ≈7% for the two-particle size fit).

Our analysis of the cluster size distributions at steady state for different Γ's provides an estimate of the solubility of B atoms in the A-rich matrix during irradiation. The results of such analysis are shown in Fig. 17, where the graphs of integrated fraction of isolated B atoms and precipitated B in all clusters smaller than size N are plotted as a function of N. Based on these dependencies, the dissolved fraction of B-rich phase in A matrix can be calculated as a function of Γ. Since a continuous transition in magnetic properties is expected, going from isolated nonmagnetic Co atoms to large superparamagnetic clusters, we assume that Co clusters composed of only a few atoms are in solution. Since the precise value for this transition cluster size is unknown, we plot two solubility curves, one including both isolated B atoms and B clusters of two atoms, and another including isolated B atoms and all B clusters with sizes up to 10 atoms (inset of Fig. 17). This graph demonstrates that the effective solubility deduced from the experiments depends rather strongly on the magnetic properties of the smallest clusters due to their relatively high populations, particularly for cases with large γ. For the steady state with Γ=100, for example, an increase in the magnetic threshold from two B atoms to ten-atom clusters results in a twofold increase in the dissolved fraction of B atoms, from 30–60 % (i.e., solubilities increasing from 3–6 %).

IV. DISCUSSION AND CONCLUSIONS

This study examined the nature of phase separation in $Cu_{1-x}Co_x$ alloys during ion irradiations. The primary issues concerned the existence of steady state microstructures, compositional patterning and the details of the dynamic phase diagram of the $Cu_{1-x}Co_x$ alloy system. Magnetic measurements were employed to measure the size of Co precipitates and the Co solubility in a Cu matrix. In addition, KMC simulations were performed on a model system, comparable to $Cu_{90}Co_{10}$ to determine a "theoretical" dynamic phase diagram for this system. The simulations, however, contain few of the complexities of real alloys, such as grain boundaries and dislocations, as well as the possibly important role of

interstitial atoms that are produced by irradiation. Thus, a comparison between the experimental results and the simulations provide a test for the robustness of the KMC model, and more generally for our understanding of phase separation alloys under irradiation.

The first important result of the experimental study is that, indeed, the $Cu_{1-x}Co_x$ alloys ($x=10$ or 15) approach steady state sizes over a wide range of temperatures, $RT < T < 330\ ^\circ C$. For the $Cu_{90}Co_{10}$ alloy the size increases from ≈ 2000 atoms (diameter ≈ 3.4 nm) at RT to ≈ 9000 atoms (diameter ≈ 5.7 nm) at 300 °C. For the $Cu_{85}Co_{15}$ alloy, the sizes increase to a slightly larger value $\approx 10\,000$ atoms (diameter=5.9 nm) at 270 °C, before macroscopic coarsening begins. Above 350 °C the sizes appear to continue to grow, although we cannot entirely exclude the possibility that they reach a steady state at some much higher dose. Our measurements are also not conclusive on whether complete solid solutions are formed during irradiation at 80 K. For the $Cu_{90}Co_{10}$ alloy, the magnetization was too small to measure, indicating complete solubility. For the $Cu_{85}Co_{15}$ alloy measured at 100 K, a small magnetization is observed ($M_S/M_T \approx 0.2$), but this can be due to either magnetic interactions of Co in solution, or very small clusters forming during warming to 300 K.

The above precipitate sizes are all based on measurements at 300 K. The value for the $Cu_{90}Co_{10}$ alloy irradiated at room temperature was obtained by scaling the 100 K measurement to 300 K using Fig. 10. While the primary purpose of this work has been to test the predictions of the dynamic phase diagram in Fig. 1, which does not depend on the actual size of the precipitates, it is useful to assess the accuracy of the magnetic measurements in view of the uncertainties arising from magnetic interactions. The absolute values are also of interest for a quantitative comparison with the KMC simulations. Past studies of magnetic interactions on $Cu_{90}Co_{10}$ alloys[18] have shown that these interactions are weak at 300 K, and that small Co precipitates in such samples behave as nearly ideal superparamagnets. The estimated error in Ref. 14 is less than a factor of 2 in particle volume (25% in diameter). This general conclusion was also obtained by Lopez *et al.* from a study comparing the precipitate sizes in $Cu_{90}Co_{10}$ alloys determined by magnetic measurements and transmission electron microscopy (TEM),[24] although uncertainties in the TEM measurements were a factor of ≈ 2 in diameter. We can also provide a rough estimate of the maximum possible errors from our measurements on our $Cu_{85}Co_{15}$ samples. The 300 K measurements on samples irradiated to high doses at 400 °C show no signs of magnetic blocking. The average sizes of these particles are $\approx 17\,000$ atoms using a two-particle size fit. The two sizes obtained from the fit were ≈ 3900 and 29 000. Since particle blocking at 300 K is expected for sizes greater than $\approx 90\,000$ atoms, the maximum error is a factor of ≈ 3 in volume. On the other hand, the particle blocking at 100 K occurs at sizes of $\approx 30\,000$ atoms, which is about the size of larger particles in the two particle size fit. Since some particles will be larger than this value, we expect some indication of particle blocking in our 100 K measurements, and indeed we find a weaker growth law for the 100 K measurements. If the particle size was much higher than our estimate, moreover, a large remanent magnetization should have been observed in the low-temperature measurements, but it was not. It appears, therefore, that the uncertainties in our sizes arising from magnetic interactions are not larger than a factor of ≈ 2 in particle volume.

The dynamic phase diagram in Fig. 1 employs γ as the control variable, not temperature. We can estimate γ using the radiation-enhanced diffusion data of Naundorf *et al.*[13] for Ni in Cu, by comparing diffusion arising from ion beam mixing and diffusion at a given temperature. At 80 K, $\gamma \rightarrow \infty$ since diffusion is due entirely to ion beam mixing. By 270 °C γ decreases to ≈ 0.1, with the decrease occurring mostly between RT and 150 °C. At temperatures between 150 and 270 °C, the results in Ref. 13 show a nearly constant diffusion coefficient. This agrees with our results for both the $Cu_{90}Co_{10}$ and $Cu_{85}Co_{15}$ alloys; the sizes of the precipitates change very little in this temperature range. Radiation-enhanced diffusion measurements above 270 °C are not currently unavailable on this system, but we note that density of defect clusters, in the form of dislocation loops, decreases rapidly with temperature beginning at $\approx 300\ ^\circ C$.[25] The loss of defect clusters, which are sinks for migrating point defects, would give rise to a large increase in the radiation-enhanced diffusion coefficient, and hence a significant reduction in γ. This would explain why the system crosses the phase boundary to macroscopic coarsening somewhat above $\approx 300\ ^\circ C$. Radiation-enhanced diffusion measurements above 270 °C, however, are clearly needed.

We lastly consider the solubility of Co in Cu. As noted above, the magnetic moment of small Co clusters and precipitates in Cu is not precisely known, but it is expected to decrease below the value $1.7\mu_B$/atom with decreasing cluster size below ~ 10 atoms. If we make the assumption that particles are in solution if they are not superparamagnetic, then the data show that the dissolved fraction in the region of patterning decreases as a function of irradiation temperature from $\approx 80\%$ at RT, 60% at 270 °C, and $\approx 40\%$ at 330 °C. In the region of continuous growth, the dissolved fraction decreases further, to $\approx 25\%$ at 400 °C. These results are in good qualitative agreement with KMC simulations. With the assumption that particles containing less than 10 Co atoms are in solution, it can be seen for the $A_{90}B_{10}$ alloy that the dissolved fraction decreases from ≈ 60 to ≈ 8 % in the region of patterning, i.e., Γ decreasing from 70 to 3. We cannot explain presently why the dissolved fractions of Co are smaller in the KMC simulations than the measured ones, but part of the reason must derive from our inexact knowledge of the magnetic properties of small clusters and our approximate method for determining the region of patterning. Another possibility is that Co atoms are trapped in small immobile defect clusters that are not fully magnetic. The clusters thus behave magnetically as if they were in solution. Such trapping reactions are not presently included in the KMC simulations. Despite this quantitative discrepancy between KMC and experiments, it is quite clear that in the regions of patterning and continuous growth, a considerable fraction of the Co remains in solution. In a similar context, we note that even when compositional patterning is clearly observed, the size distribution of clusters is quite broad in the KMC simu-

lations. The need for a two particle-size fit in the magnetic data suggests that the experimental distribution of sizes is similarly broad.

Finally we summarize the main conclusions of this work as follows.

(1) Prolonged irradiation of $Cu_{1-x}Co_x$ alloys with MeV Kr ions, for $x=10$, 15, and 20 %, leads to steady state microstructures for T less than $\approx 330\ ^\circ C$.

(2) Between RT and $\approx 330\ ^\circ C$ (γ ranging from ≈ 1 to ≈ 0.1) these alloys show mesoscopic patterning, in that a specific steady state size distribution of precipitates develops. For $Cu_{90}Co_{10}$ the average volume weighted size is ≈ 2000 atoms at RT and ≈ 9000 atoms at $300\ ^\circ C$. Steady state sizes for $Cu_{85}Co_{15}$ at $270\ ^\circ C$ is $\approx 10\,000$ atoms. Strong interference of magnetic interactions between the particles and blocking prevented a similar determination for $Cu_{80}Co_{20}$.

(3) At temperatures greater than $330-350\ ^\circ C$ the sizes of the precipitates do not saturate with dose, signaling the transition into the regime of macroscopic growth. At the lowest temperature probed in this study (LNT), the state of random solution is reached. The onset of macroscopic growth at $330\ ^\circ C$ coincides, approximately, with a dramatic decrease in production of dislocation loops in energetic displacement cascades.

(4) KMC simulations on a model system resembling $Cu_{90}Co_{10}$ are in good qualitative agreement with the experiments, showing the existence of the three regimes of microstructure evolution with irradiation dose: patterning, macroscopic growth, and solid solution. The simulations, however, do not show a good quantitative agreement with the experiments, the maximum particle size in simulations being ≈ 2500 atoms compared to ≈ 9000 in the experiments. The transition between the patterning and macroscopic growth regimes appears to be a first-order transition, while the transition from pattering to random solution is smooth, characterized by a gradual decrease in the average steady-state size of Co particles.

ACKNOWLEDGMENTS

This work was supported by the U.S. Deptartment of Energy, Basic Energy Sciences, under Grant No. DEFG02-91ER45439, and in part by the National Science Foundation under Grant No. NSF DMR0407958. The experiments were carried out in the Center for Microanalysis of Materials, University of Illinois, which is partially supported by the U.S. Department of Energy under Grant No. DEFG02-91-ER45439.

[1] See, e.g., A. Meldrum, L. A. Boatner, and C. W. White, Nucl. Instrum. Methods Phys. Res. B **178**, 7 (2001), and references therein.
[2] J. R. Childress and C. L. Chien, J. Appl. Phys. **70**, 5885 (1991).
[3] R. A. Enrique and P. Bellon, Phys. Rev. B **60**, 14 649 (1999).
[4] R. A. Enrique and P. Bellon, Phys. Rev. Lett. **84**, 2885 (2000).
[5] K. H. Heinig, T. Muller, B. Schmidt, M. Strobel, and W. Moller, Appl. Phys. A: Mater. Sci. Process. **77**, 17 (2003).
[6] G. Martin, P. Bellon, Solid State Phys. **50**, 189 (1997).
[7] P. Bellon and R. S. Averback, Scr. Mater. **49**, 921 (2003).
[8] R. A. Enrique and P. Bellon, Phys. Rev. B **63**, 134111 (2001).
[9] S. Zghal, P. Bhattacharya, R. Twesten, F. Wu, and P. Bellon, Mater. Sci. Forum **386–388**, 165 (2002); F. Wu, P. Bellon, A. J. Melmed, and T. A. Lusby, Acta Mater. **49**, 453 (2001).
[10] I. S. Servi and D. Turbull, Acta Metall. **14**, 161 (1966).
[11] R. A. Enrique, K. Nordlund, R. S. Averback, and P. Bellon, J. Appl. Phys. **93**, 2917 (2003).
[12] R. S. Averback and Diaz de la Rubia, Solid State Phys. **51**, 281 (1998).
[13] V. Naundorf, M.-P. Macht, H.-J. Gudladt, and H. Wollenberger, in *Point Defects and Defect Interactions in Metals*, edited by J.-I. Takamura, M. Doyama, and M. Kiritani (University of Tokyo Press, Tokyo, 1982), p. 934.
[14] J. J. Becker, Trans. AIME **209**, 59 (1957).
[15] C. P. Bean and J. D. Livingston, J. Appl. Phys. **30**, 120S (1959).
[16] R. von Helmolt, J. Wecker, and K. Samwer, Phys. Status Solidi B **182**, K25 (1994).
[17] R. H. Yu, X. X. Zhang, J. Tejada, M. Knobel, P. Tiberto, and P. Allia, J. Phys.: Condens. Matter **7**, 4081 (1995).
[18] P. Allia, M. Coisson, J. Moya, P. Tiberto, and F. Vinai, J. Magn. Magn. Mater. **254–255**, 143 (2003).
[19] G. Martin, Phys. Rev. B **30**, 1424 (1984).
[20] P. Allia, M. Coisson, P. Tiberto, F. Vinai, M. Knobel, M. A. Novak, and W. C. Nunes, Phys. Rev. B **64**, 144201 (2001).
[21] Approximately 2% of the sample is sputter-eroded during the irradiation. Moreover, since Co has a smaller atomic size than Cu, it is likely to segregate to the surface, making the fractional loss of Co much higher than a few percent.
[22] We show later that magnetic measurements performed at 100 K underestimate the true size by factor of about 3.
[23] F. H. Stillinger and T. A. Weber, Phys. Rev. B **31**, 5262 (1985).
[24] A. Lopez, F. J. Lazaro, R. von Helmolt, J. L. Garcia-Palacios, J. Wecker, and H. Cerva, J. Magn. Magn. Mater. **187**, 221 (1998).
[25] T. L. Daulton, M. A. Kirk, and L. E. Rehn, Philos. Mag. A **80**, 809 (2000).